Power Electronic Systems
Laboratory

Proceedings of the IEEE Energy Conversion Congress and Exposition (ECCE USA 2013), Denver, Colorado, USA,
September 15-19, 2013

Weight Optimization of a Cooling System Composed of Fan and Extruded Fin Heat Sink

C. Gammeter,
F. Krismer,
J. W. Kolar

Eidgenössische Technische Hochschule Zürich
Swiss Federal Institute of Technology Zurich

Weight Optimization of a Cooling System Composed of Fan and Extruded Fin Heat Sink

Christoph Gammeter, Florian Krismer and Johann W. Kolar
Power Electronic Systems Laboratory
Swiss Institute of Technology,
Physikstrasse 3
8092 Zurich, Switzerland

***Abstract*—This Paper details the weight optimization of forced convection cooling systems, composed of fan and extruded fin heat sink, required for a dc–dc converter of an airborne wind turbine (AWT) system. The presented investigations detail the optimization of the heat sink's fins with respect to minimum weight and the selection of a suitable fan for minimum overall system weight. A new analytical cooling system model is introduced, the calculated results are compared to the results determined with a preexisting analytical model and Finite Element Model (FEM) simulations. The comparison to experimental results demonstrate the accuracy improvements achieved with the proposed methods. Compared to commercially available products a weight reduction of 52 % is achieved with the proposed optimization procedure for the required heat sink system with $R_{\text{th,S-a}} = 1\,\text{K/W}$.**

I. Introduction

Increasing consumption of electric energy, environmental issues, and limited availability of fossil fuels have led to a multitude of developments related to the generation of electricity from renewable energy sources. One innovative system in this context is the airborne wind turbine (AWT) detailed in [1], which generates electricity from high altitude winds. High altitude winds are known to be more stable and faster than winds close to ground-level and, thus, enable a more reliable and effective generation of electric energy [1].

The AWT is essentially a flying wing with a significantly lower construction effort of the power generation system compared to a traditional wind turbine. A long fiber and cable combination (tether $\approx 1\,\text{km}$ long) ties the AWT to the ground and, additionally, provides the electrical link to the ground station [1].

The greatest challenge with respect to the realization of the electric system of the AWT is to achieve a light-weight tether and light-weight generators and power converters. The considered AWT system is rated for a maximum input power of $100\,\text{kW}$ and related investigations detailed in [1] reveal that a low-weight realization of this AWT makes a dc–dc converter necessary, which boosts the dc bus voltage, V_1, on-board the AWT ($650\,\text{V} < V_1 < 750\,\text{V}$) to a high tether voltage of up to $8\,\text{kV}$, cf. Fig. 1. The tether voltage is set to $V_2 = 8\,\text{kV}\ V_1/750\,\text{V}$, i.e. $V_2/V_1 = 8\,\text{kV}/750\,\text{V} \approx 10.7$ since the dc–dc converter is operated most efficiently with constant conversion ratio. The dc–dc converter further needs to allow for bi-directional energy transfer in order to enable the start-up of the AWT, where the rated power is $100\,\text{kW}$.

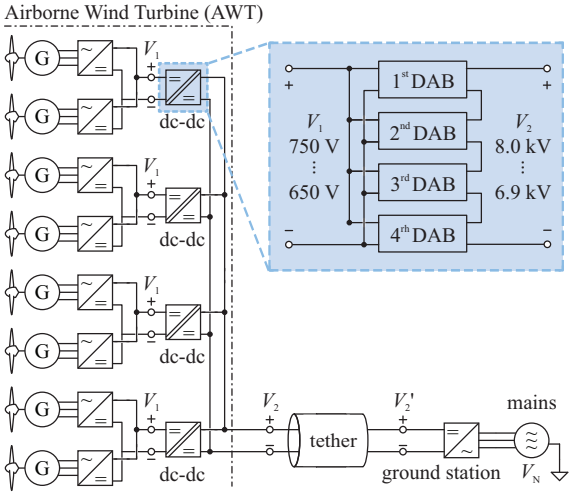

Fig. 1. Electrical system of the airborne wind turbine (AWT). Four bi-directional dc–dc converters link eight voltage source rectifiers, to a tether and power transmission tether ($\approx 1\,\text{km}$). The ground station, i.e. bi-directional dc–ac converter, connects the tether to the three-phase grid. Four single converter cells form a bi-directional dc–dc converter with a dc port voltage V_2 of up to $8\,\text{kV}$.

Fig. 1 depicts the electrical system of the AWT proposed in [1]: eight voltage source rectifiers convert the ac voltage of the generators to dc; four bi-directional dc–dc converters generate the high tether voltage; and the ground station, connects the tether to the three-phase grid on the ground. The converter topology for the dc–dc converter is detailed in [2]. Each converter is formed by four single cells that are connected in parallel on the low voltage side and in series on the high voltage side in order to reduce the maximum tether side port voltage of each converter cell to $2\,\text{kV}$. Each converter cell essentially is a dual active bridge (DAB) converter with a full bridge circuit on the low voltage side (dc port voltage V_1), a high frequency (hf) transformer and inductor, and a neutral point clamped (NPC) circuit on the high voltage side [dc port voltage $V_{2,i}$, Fig. 2]. The optimization of the dc–dc converter with respect to minimum weight is particularly related to the optimization of the cooling system (heat sink plus fan), since the cooling system in a large part contributes to the total converter weight [1].

An optimization of heat sinks with respect to minimum

978-1-4799-0336-8/13/$31.00 ©2013 IEEE

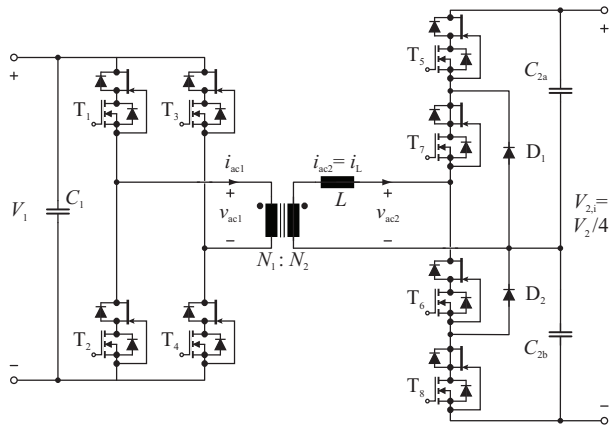

Fig. 2. A modified dual active bridge (DAB) converter topology is used to realize a single cell of the bi-directional dc–dc converter [2].

weight, based on FEM, and a comparison of different materials suitable for low-weight heat sinks are presented in [3]. This optimization, however, considers only natural convection. Furthermore, the heat sink optimization presented in this work is part of an overall converter optimization procedure and, thus, analytical expressions for the expected thermal resistance (heat sink to ambient), rather than FEM simulation results, are desirable in order to increase the evaluation speed.

Optimization procedures for complete cooling systems with respect to minimum thermal resistance are discussed in [4]–[6]. Lee, [4], outlines the general optimization problem and the impacts of different parameter variations (e.g. fin thickness) on the resulting thermal resistance values. Holahan, [5], refines the thermal model of the heat sink and includes the fan characteristic (static pressure versus volume flow) in the heat sink optimization. Finally, Drofenik, [6], presents a complete heat sink optimization procedure. The optimizations in [5] and [6] minimize thermal resistance in order to minimize the cooling system volume, the weight of the system is not considered.

This paper presents a modified optimization procedure that yields a minimum weight cooling system. It is based on analytical expressions and requires comparably low computational effort. Thus, the proposed procedure can directly be used as part of a complete converter weight optimization routine. Section II details a analytical cooling system model. Section III presents a comparison of the results obtained from FEM simulation, the model of [6], and the proposed analytical model. Section IV details the proposed optimization procedure. Section V, finally, discusses experimental result.

II. Cooling System Model

Thermal modeling of a heat sink with fan is a multi–physics problem. The thermal modeling involves three domains, heat conduction in solids, convective heat and mass transfer, and hydrodynamics. Section II-A covers heat conduction and convective heat and mass transfer. Section II-B covers the hydrodynamics.

The proposed optimization procedure in Section IV considers a cooling system with heat sink and fan, and extends a conventional heat sink geometry, defined in Fig. 3(a), with an air duct, shown in Fig. 3(b). It further considers closed heat sink channels in order to avoid a degradation of the heat sink's thermal resistance due to flow bypass [4]. The considered thermal model, depicted in Fig. 3(c), assumes equal fin spacing s and fin thickness t with n channels. Therefore, and due to symmetry conditions, only one channel/fin is modeled.

A. Thermal Model

A simple way to model the three dimensional heat conduction problem is to represent the three dimensional structure as a network of thermal resistances. To keep the thermal network as simple as possible the heat sink symmetries can be exploited, resulting in a thermal resistance network as shown Fig. 3(c). The thermal resistances $R_{\text{th,d}}$ is a function of the heat sink geometry and the heat sink materials thermal conductivity λ_{hs},

$$R_{\text{th,d}} = \frac{d}{bL\lambda_{\text{hs}}}. \tag{1}$$

$R_{\text{th,fin}}$, $R_{\text{th,A}}$, $R_{\text{th,a}}$ and T_{channel} are nonlinear functions of volume flow $\dot{V}$ and geometry. This is most appropriately modeled as a single fluid heat exchanger as discussed in [7], [8]. If the average heat transfer coefficient h is known the total thermal resistance is

$$R_{\text{th,S-a}} = R_{\text{th,d}} + \frac{1}{\rho_{\text{air}} c_{\text{air}} \dot{V} \left[1 - e^{-\frac{h A_{\text{eff}}}{\rho_{\text{air}} c_{\text{air}} \dot{V}}}\right]}, \tag{2}$$

with the effective surface area and fin efficiency [9],

$$A_{\text{eff}} = n(2c\eta + s)L \text{ and } \eta = \frac{\tanh\left(\sqrt{\frac{h2(t+L)}{\lambda_{\text{hs}} tL}} \cdot c\right)}{\sqrt{\frac{h2(t+L)}{\lambda_{\text{hs}} tL}} \cdot c}. \tag{3}$$

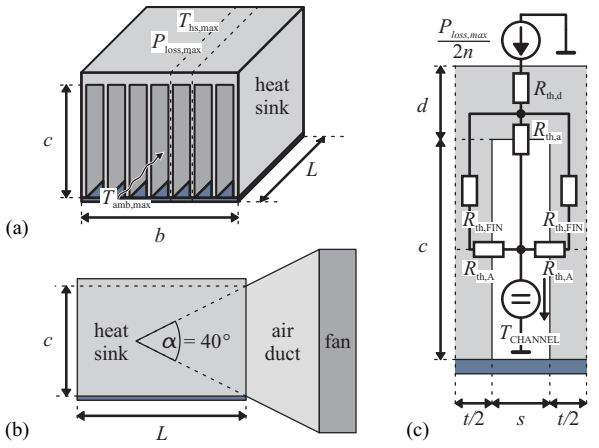

Fig. 3. (a) Geometrical model of heat sink; the bottom plate (made of PVC) prevents flow bypass and the dotted lines indicate the symmetry axes used for the thermal model. (b) Cooling system model for fin length optimization with air duct; for the air duct a fixed angle $\alpha = 40\,^\circ$ is considered. (c) Heat sink thermal model, due to symmetry properties only two half fins left and right to a channel, $t/2$, and one channel, s, need to be considered [6].

Expressions (2) and (3) assume that the average heat transfer coefficient, h, is known. The average heat transfer coefficient is predominantly a function of the fluid boundary layer velocity. For viscous flow in ducts this boundary layer velocity is a function of the average fluid velocity in the duct and the fluid viscosity ν_{air}, which is generally describe by means of non-dimensional analysis and the use of the Nusselt number. The Nusselt number however is a function of average duct velocity, geometry and the Prandtl number, Pr. Muzychka and Yovanovich have derived an analytical model for the Nusselt number, $\text{Nu}_{\sqrt{A}}$, suitable for the extruded fin heat sink model, which includes the effect of flow development at the inlet of a duct with arbitrary cross section [10]:

$$\text{Nu}_{\sqrt{A}} = \left[\left(\frac{C_4 f(\text{Pr})}{\sqrt{z^\star}} \right)^m + \left(\left\{ C_1 \left(\frac{f\text{Re}_{\sqrt{A}}}{8\sqrt{\pi}\epsilon^\gamma} \right) \right\}^5 + \left\{ C_2 C_3 \left(\frac{f\text{Re}_{\sqrt{A}}}{z^\star} \right)^{1/3} \right\}^5 \right)^{m/5} \right]^{1/m}. \quad (4)$$

At the inlet of the duct the velocity profile of the boundary layer shows a distinct dependency on the position along the axis perpendicular to the front surface. As a consequence, the Nusselt number is large at the inlet of the duct, where the boundary layer velocity is large. The Nusselt number decreases along the thermal entry length, [8], and settles to a constant value. The model developed in [10] describes this effect and is solved for uniform wall flux (UWF) and uniform wall temperature (UWT) boundary conditions. The presented investigation assumes UWT, due to the high thermal conductivity of the heat sink material. For UWT boundary conditions the function $f(\text{Pr})$ is

$$f(\text{Pr}) = \frac{0.564}{[1 + (1.664\ \text{Pr}^{1/6})^{9/2}]^{2/9}} \quad (5)$$

and the parameters C_1 and C_3 are $C_1 = 3.24$ and $C_3 = 0.409$, given in [10]. To calculate the average (not local) Nusselt number the parameters C_2 and C_4 are $C_2 = 3/2$ and $C_4 = 2$. The shape factor is $\gamma = -3/10$ for rectangular ducts. The blending parameter m is given by

$$m = 2.27 + 1.65\ \text{Pr}^{1/3}. \quad (6)$$

The model of [10] is valid for $0.1 < \text{Pr} < \infty$, which is valid for most heat exchanger applications. For the extruded fin heat sink the shape functions are

$$z^\star = \frac{L n \nu_{\text{air}}}{\text{Pr} \cdot \dot{V}} \text{ and } \epsilon = \frac{s}{c} \leq 1. \quad (7)$$

The friction factor Reynolds product function

$$f\text{Re}_{\sqrt{A}} = \left[\frac{11.8336 \cdot \dot{V}}{L n \nu_{\text{air}}} + \left(f\text{Re}_{\sqrt{A},\text{fd}} \right)^2 \right]^{1/2} \quad (8)$$

$$f\text{Re}_{\sqrt{A},\text{fd}} = \frac{12}{\sqrt{\epsilon}(1+\epsilon)\left[1 - \frac{192}{\pi^5}\epsilon \tanh\left(\frac{\pi}{2\epsilon}\right)\right]} \quad (9)$$

describes the boundary layer velocity profile and is the hydrodynamic friction factor for developing viscous flow in ducts covered in the next section. The heat transfer coefficient then becomes

$$h = \frac{\text{Nu}_{\sqrt{A}} \lambda_{\text{air}}}{d_{\text{h}}} \text{ with } d_{\text{h}} = \frac{2sc}{s+c} \text{ and } s = \frac{b-(n+1)t}{n}. \quad (10)$$

With the approximation of the average heat transfer coefficient h the total thermal resistance can be calculated as a function of geometry and volume flow $\dot{V}$.

Fig. 4 shows the thermal resistance model in [6] (green line), the proposed model (red line) and FEM simulation results, for one cooling system geometry. The thermal resistance of the FEM simulations were calculate for maximum base plate temperature (solid blue line) and minimum base plate temperature (dottet blue line). A comparison reveals, that the model in [6] significantly overestimates the thermal resistance for low volume flows. The discontinuity in the model given in [6] is caused by the discrete distinction between laminar and turbulent flow ($\text{Re} > 2300$) and the use of the turbulent flow model within the transition region ($2300 < \text{Re} < 5000$). The distinction between turbulent and laminar flow is essential for fully developed fluid flow. This distinction however only becomes valid once the hydrodynamic entry length has been reached, where the fluid flow turns from laminar to turbulent [11]. For the cooling system geometry in Fig.4 the hydrodynamic entry length [8]

$$L_{\text{h}} = \frac{L_{\text{h}}^+}{\sqrt{A}} \text{Re}_{\sqrt{A}} = L_{\text{h}}^+ \frac{\dot{V}}{n\nu_{\text{air}}}, \quad (11)$$

with the dimensionless hydrodynamic entry length for laminar flow [8]

$$L_{\text{h}}^+ = 0.0822\epsilon(1+\epsilon)^2 \left[1 - \frac{192\epsilon}{\pi^5} \tanh\left(\frac{\pi}{2\epsilon}\right)\right], \quad (12)$$

is $L_{\text{h}} = 650\,\text{mm}$ at $\text{Re} = 2300$ and $L_{\text{h}} = 1425\,\text{mm}$ at $\text{Re} = 5000$. Therefore turbulent flow will not develop over the whole length $L = 100\,\text{mm} \ll L_{\text{h}}$ of the heat sink presented in this work.

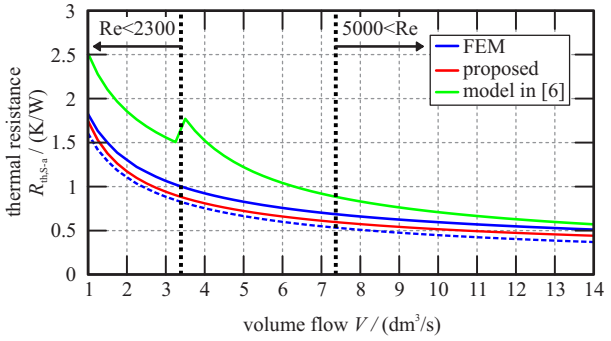

Fig. 4. Thermal resistance $R_{\text{th,S-a}}$ as a function of volume flow $\dot{V}$: FEM calculated with maximum base plate temperature (solid blue), FEM calculated with minimum base plate temperature (dotted blue), proposed model (red), model proposed in [6] (green), for a heat sink with dimensions $n = 5$, $L = 100\,\text{mm}$, $b = 40\,\text{mm}$, $d = 3\,\text{mm}$, $c = 30\,\text{mm}$, $t = 1\,\text{mm}$.

B. Hydrodynamic Model

The sole purpose of the hydrodynamic model is to determine the volume flow $\dot{V}$, which is an input of the thermal model [in particular (2)], generated by the selected fan. Literature review reveals that different phenomena affect the relation between the total static pressure drop Δp_{tot} and the volume flow for a given heat sink. All these effects are functions of the geometry and average air speed. In [6] only the friction factor for fully developed flow between two parallel plates is considered, which, however, turns out to insufficiently predict the actual pressure drop and volume flow, since the criteria required for approximation of the friction factor as the friction factor for fully develop fluid flow $L_{\text{fd}}^{+} \approx 10 L_{\text{h}}^{+}$ is not fulfilled in commonly used heat sink geometries [8]. Improved fluid dynamic models are proposed in [12]–[14]. Reference [12] and [13] include the effects of sudden contraction at the inlet and sudden expansion at the outlet, based on [11], and the effects of developing flow [14].

Further, the conservation of momentum needs to be considered in order to account for the fluid acceleration in the air duct and the heat sink. Respective literature is found in [11], [15]–[17].

The total cooling system static pressure drop then becomes the sum of all the pressure drop contributions expressed as functions of volume flow,

$$\Delta p_{\text{tot}}(\dot{V}) = \Delta p_{\text{hs}}(\dot{V}) + \Delta p_{\text{duct}}(\dot{V}) + \Delta p_{\text{acc}}(\dot{V}). \tag{13}$$

The heat sink static pressure drop,

$$\Delta p_{\text{hs}}(\dot{V}) = \left(f_{\text{app}}(\dot{V}) \frac{L}{d_h} + K_{\text{se}} + K_{\text{sc}} \right) \cdot \frac{\rho}{2} \overline{U}_{\text{hs}}^2(\dot{V}), \tag{14}$$

consists of the friction factors for sudden contraction and sudden expansion [11], [12], [17],

$$K_{\text{se}} = \left(1 - \frac{d_h^2}{D_h^2}\right)^2 = \left(1 - \left(1 - \frac{(n+1)t}{b}\right)^2\right)^2, \tag{15}$$

$$K_{\text{sc}} \approx 0.42 \left(1 - \frac{d_h^2}{D_h^2}\right) = 0.42 \left(1 - \left(1 - \frac{(n+1)t}{b}\right)^2\right), \tag{16}$$

and the apparent friction factor for viscous fluid flow in ducts [14],

$$f_{\text{app}}(\dot{V}) = \frac{f\text{Re}_{\sqrt{A}}(\dot{V})}{\text{Re}_{\sqrt{A}}(\dot{V})} = \frac{n\nu\sqrt{cs}}{\dot{V}} \cdot f\text{Re}_{\sqrt{A}}(\dot{V}). \tag{17}$$

The air duct static pressure drop,

$$\Delta p_{\text{duct}}(\dot{V}) = \left(f_{\text{app,duct}}(\dot{V}) \frac{L_{\text{duct}}}{\overline{d}_{\text{h,duct}}} \frac{1}{4} + K_{\text{venturi}} \right) \cdot \frac{\rho}{2} \overline{U}_{\text{duct}}^2(\dot{V}) \tag{18}$$

consists of the apparent friction factor for the average duct hydraulic diameter and the friction factor for a venturi nozzle [11], [14], [16],

$$f_{\text{app,duct}}(\dot{V}) = \frac{f\text{Re}_{\sqrt{A}}(\dot{V})}{\text{Re}_{\sqrt{A}}(\dot{V})} = \frac{\nu\sqrt{b(b+c)}}{\sqrt{2}\dot{V}} \cdot \left[\frac{11.8336 \dot{V} 2 \tan(\alpha)}{(b-c)\nu} + \left(f\text{Re}_{\sqrt{A},\text{fd}}\right)^2 \right]^{1/2} \tag{19}$$

$$\overline{d}_{\text{h,duct}} = \frac{2b(b+c)}{3b+c}, \; L_{\text{duct}} = \frac{b-c}{2\tan(\alpha)}, \; \epsilon_{\text{duct}} = \frac{b+c}{2c}, \tag{20}$$

$$K_{\text{venturi}} \approx 0.2. \tag{21}$$

The average velocities are given as functions of volume flow,

$$\overline{U}_{\text{hs}}(\dot{V}) = \frac{\dot{V}}{nsc} \text{ and } \overline{U}_{\text{duct}}(\dot{V}) = \frac{\dot{V}}{bc}. \tag{22}$$

Conservation of momentum for the air duct and heat sink [11], [15]–[17], gives the pressure drop for the frictionless fluid flow acceleration,

$$\Delta p_{\text{acc}}(\dot{V}) = \left(\frac{1}{(nsc)^2} - \frac{1}{(b^4)} \right) \cdot \frac{\rho}{2} \dot{V}^2 \; . \tag{23}$$

Fig. 5 shows the contributions of the different effects causing the total heat sink static pressure drop (red line), for an example cooling system with dimensions $n = 5$, $L = 100\,\text{mm}$, $b = 40\,\text{mm}$, $d = 3\,\text{mm}$, $c = 30\,\text{mm}$, $t = 1\,\text{mm}$. The shaded areas from bottom to top are: apparent friction factor f_{app}, sudden expansion K_{se}, sudden contraction K_{sc}, conservation of momentum Δp_{acc} and the friction factor of the duct Δp_{duct}.

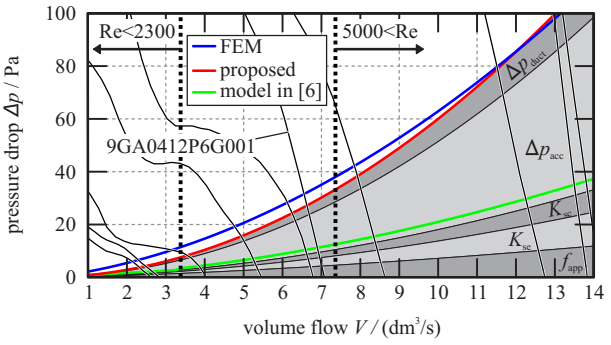

Fig. 5. Cooling system static pressure drop Δp_{tot} as a function of volume flow $\dot{V}$, FEM (blue), proposed model (red), model proposed in [6] (green), for a heat sink with dimensions $n = 5$, $L = 100\,\text{mm}$, $b = 40\,\text{mm}$, $d = 3\,\text{mm}$, $c = 30\,\text{mm}$, $t = 1\,\text{mm}$. The shaded areas from bottom to top show the contributions of apparent friction factor f_{app}, sudden expansion K_{se}, sudden contraction K_{sc}, conservation of momentum Δp_{acc} and the friction factor of the duct Δp_{duct}. The static pressure drop characteristics of the fans in Tab. I are superimposed in black.

Fig. 5 further shows the hydrodynamic model proposed in [6] (with fitting factor k, green line) and FEM simulation results (blue line), the horizontal dotted lines indicate the boundaries for laminar ($\text{Re} < 2300$) and turbulent flow ($5000 < \text{Re}$).

Fig. 5 shows that the friction factor Reynolds product $f\text{Re}_{\sqrt{A}}$, which is essential for the calculation of the average heat transfer coefficient, is only a minor contributions to the total static pressure drop characteristic of the cooling systems considered in this work.

III. Model Comparison

The proposed thermal and hydrodynamic model and the model proposed in [6] are compared to FEM simulation results (in COMSOL Multiphysics) and, in Section V, to

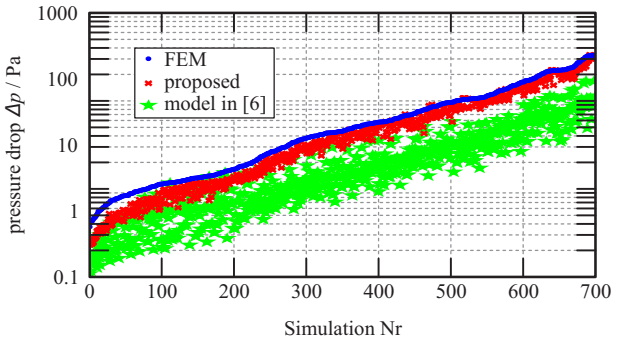

Fig. 6. Comparison of the total static pressure drop Δp_{tot} at the operating points of the fans listed in Tab. I. The geometry parameters of the considered cooling systems are in the range of $L \in [60\,\text{mm},100\,\text{mm}]$, $n \in [5, 13]$, $c \in [10\,\text{mm},37\,\text{mm}]$, $b = [40\,\text{mm}]$, $t = [1\,\text{mm}]$. FEM simulation (blue dot), cooling system model proposed in [6] (green star) and new cooling system model (red cross).

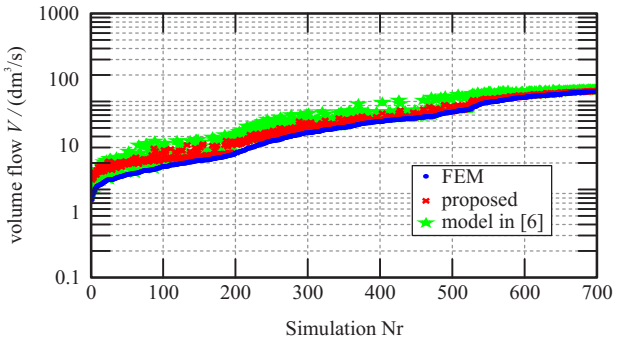

Fig. 7. Comparison of the static volume flow $\dot{V}$ at the operating points of the fans listed in Tab. I.The geometry parameters of the considered cooling systems are in the range of $L \in [60\,\text{mm},100\,\text{mm}]$, $n \in [5, 13]$, $c \in [10\,\text{mm},37\,\text{mm}]$, $b = [40\,\text{mm}]$, $t = [1\,\text{mm}]$.. FEM simulation (blue dot), cooling system model proposed in [6] (green star) and new cooling system model (red cross).

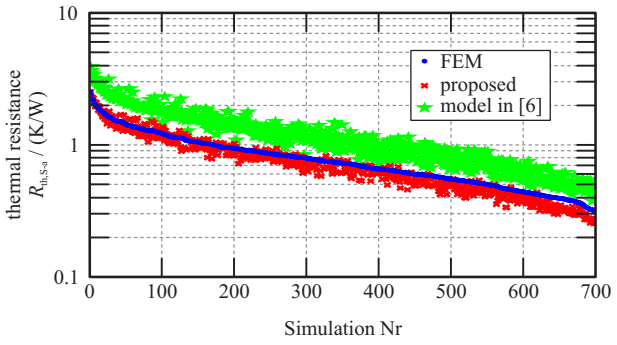

Fig. 8. Comparison of the thermal resistance values $R_{\text{th,S-a}}$ at the operating points of the fans listed in Tab. I determined by the FEM model.The geometry parameters of the considered cooling systems are in the range of $L \in [60\,\text{mm},100\,\text{mm}]$, $n \in [5, 13]$, $c \in [10\,\text{mm},37\,\text{mm}]$, $b = [40\,\text{mm}]$, $t = [1\,\text{mm}]$.. FEM simulation (blue dot), cooling system model proposed in [6] (green star) and new cooling system model (red dot).

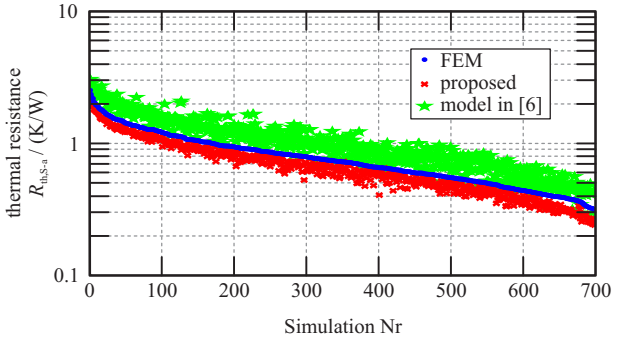

Fig. 9. Comparison of the thermal resistance values $R_{\text{th,S-a}}$ at the operating points of the fans listed in Tab. I. The geometry parameters of the considered cooling systems are in the range of $L \in [60\,\text{mm},100\,\text{mm}]$, $n \in [5, 13]$, $c \in [10\,\text{mm},37\,\text{mm}]$, $b = [40\,\text{mm}]$, $t = [1\,\text{mm}]$.. FEM simulation (blue dot), cooling system model proposed in [6] (green star) and new cooling system model (red dot).

experimental results, in order to present the achieved improvements. Assuming that the most accurate calculation of thermal resistance, volume flow, and pressure drop is feasible with FEM simulations a large number of FEM simulations is used as basis of the evaluation. The thermal resistance values of the FEM simulations are calculated with the maximum base plate temperature.

The hydrodynamic models, which determine the operating point of the fan, are needed to evaluate the thermal model, in particular (2), and are analyzed first. Fig. 6 and 7 show the calculated operating points for the considered fans in Tab. I and 72 different heat sink geometries with parameters in the range of $L \in [60\,\text{mm},100\,\text{mm}]$, $n \in [5, 13]$, $c \in [10\,\text{mm},37\,\text{mm}]$, $b = 40\,\text{mm}$, $t = 1\,\text{mm}$, and $\dot{V} \in [1\,\text{dm}^3/\text{s},14\,\text{dm}^3/\text{s}]$. The operating point is determined by equalizing the cooling system static pressure drop and the fan (the fan characteristic are obtained from data sheets). Fig. 6 – 9 and 14 the results of the FEM simulations are marked with blue dots, the results of the proposed model with red crosses and the results of the model proposed in [6] with green stars. For a better graphic representation the results in Figs. 6 – 9 are sorted in different orders, such that the blue line (FEM simulation results) is monotonic.

Fig. 6 shows a high correlation for the pressure drop of the proposed model and the FEM simulation with a mean deviation of

$$\sigma_{\Delta p_{\text{tot}}} = \frac{1}{k}\sum_{i=1}^{k}\frac{\|\Delta p_{\text{tot,FEM}} - \Delta p_{\text{tot,model}}\|}{\Delta p_{\text{tot,FEM}}} = 21\%, \qquad (24)$$

($k = 72 \cdot 10$), whereas the previous cooling system model shows a mean deviation of $\sigma_{\Delta p_{\text{tot}}} = 64.3\%$.

Fig. 7 shows the volume flow of the calculated operating points. The mean deviations between simulated and calculated results are 14.6% for the proposed model and 24.7% for the model detailed in [6].

Fig. 8 depicts the expected thermal resistances if the operating points are determined based on the pressure drop versus volume flow characteristics obtained by means of FEM simulations in order to facilitate a separate inspection of the results achieved with the analytical thermal model

of Section II-A. The mean deviations between simulated and calculated results are 9.9% for the proposed model and 45.7% for the previous model [6].

Fig. 9, finally, compares the expected thermal resistances of the combined hydrodynamic and thermal models. The mean deviations are 15% for the proposed model and 30.3% [6].

IV. Cooling System Optimization

A. General Constrained Optimization Procedure

The algorithm of the optimization procedure, illustrated in Fig. 10, yields a minimum weight cooling system and, additionally, satisfies design and manufacturability constraints. Its main input parameters are a list of considered fans, the required base plate area A_{hs} and the maximum allowable thermal resistance of the cooling system,

$$R_{\text{th,S-a,max}} = \frac{T_{\text{hs,max}} - T_{\text{amb,max}}}{P_{\text{loss,max}}}, \tag{25}$$

with maximum base plate temperature of the heat sink, $T_{\text{hs,max}}$, maximum ambient temperature specified, $T_{\text{amb,max}}$, and maximum thermal flux transmitted to the heat sink's base plate, $P_{\text{loss,max}}$.

The thickness of the base plate is set to the minimum possible value in order to achieve a low weight of the heat sink. In this work the minimum thickness is $d = 3\,\text{mm}$ in order to facilitate sufficient mechanical stability and depth for the M3 threads that are needed to mount the components onto the heat sink. Despite the thin base plate, a constant and homogeneous temperature $T_{\text{hs,max}}$ all over the surface of the base plate is considered, due to the high thermal conductivity material, i.e. Aluminum, employed. Moreover, the components mounted to the heat sink are assumed to cover large parts of the available surface, as shown in Figs. 13(a) and (b), in order to achieve a well-balanced distribution of the thermal flux across the surface of the base plate. The procedure detailed in [6] sets the height, $c+d$, and the width b of the heat sink equal to height and width of the fan employed, the air duct, however, allows for a variable fin length c and adds an additional degree of freedom. The total area requirement of all components and the arrangement on the base plate of the heat sink, defines the length of the heat sink, $L = A_{\text{hs}}/b$.

Thus, the variables remaining for optimization are: the number of channels, n, the fin thickness, t, and the fin length, c, which are constrained by the manufacturing technology available. The presented cooling systems are manufactured with CNC-machines and, thus, a minimum fin thickness of $1\,\text{mm}$ and a minimum channel width, s, of $1\,\text{mm}$ apply.

In an initial step, the optimization procedure selects a list of fans. The fan list consists of fans with equal width and contains the fan's width, height, weight, and pressure drop characteristic. Further the geometry parameters defined by the fan, i.e. b and L are set. In a second step, an outer loop

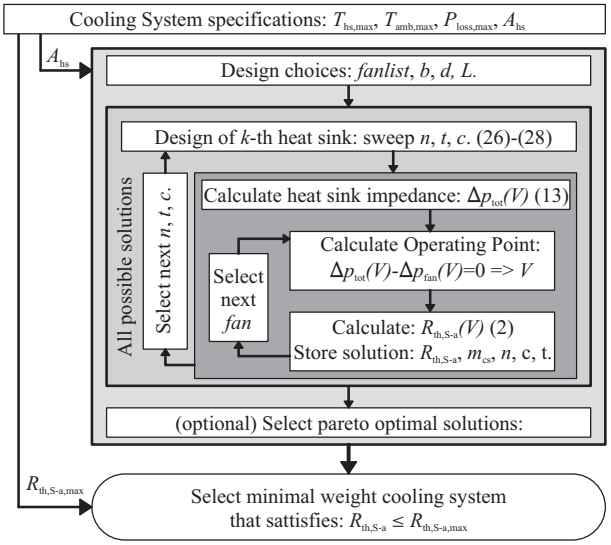

Fig. 10. Proposed cooling system optimization procedure for minimum weight cooling system that satisfies $R_{\text{th,S-a}} \le R_{\text{th,S-a,max}}$.

sweeps all possible heat sink geometries given by

$$1 \le n \le \left\lfloor \frac{b - t_{\min}}{s_{\min} + t_{\min}} \right\rfloor, \tag{26}$$

$$t_{\min} \le t \le \frac{b - n s_{\min}}{n+1}, \tag{27}$$

$$c_{\min} \le c \le b - c, \tag{28}$$

where $c_{\min}$ can be chosen arbitrarily. With the heat sink and duct geometries defined, the hydrodynamic system impedance characteristic $\Delta p_{\text{tot}}(\dot{V})$ is calculated. An inner loop calculates the operating point, of the fan, the resulting thermal resistance $R_{\text{th,S-a}}$, the weight m_{cs}, of the particular combination of heat sink and fan. The solutions are stored in a solution database.

To reduce storage space of the solution database all suboptimal solutions are excluded, i.e. exclude all solutions which feature non minimal thermal resistance $R_{\text{th,S-a}}$ for a given mass m_{cs}. The algorithm, finally, picks that particular entry of the result database, which features minimum weight and satisfies $R_{\text{th,S-a}} \le R_{\text{th,S-a,max}}$. This entry represents the optimal cooling system design (within the constraints and accuracies resulting from the list of considered fans, cf. Tab. I, and the accuracies due to limited resolutions of the sweeps (27) and (28).

The bi-directional dc–dc converter of [2] requires three cooling systems, one for the low voltage full bridge ($R_{\text{th,S-a,max,FB}} = 1.1\,\text{K/W}$), one for the medium voltage NPC converter ($R_{\text{th,S-a,max,NPC}} = 1.25\,\text{K/W}$), and one for the transformer and the inductor ($R_{\text{th,S-a,max,tr+ind}} = 0.46\,\text{K/W}$). The minimum base plate areas for the full bridge and the NPC converters are both $A_{\text{hs,min,FB}} = A_{\text{hs,min,NPC}} = 2400\,\text{mm}^2$, the minimum base plate area for inductor and transformer is $A_{\text{hs,min,tr+in}} = 3200\,\text{mm}^2$. Tab. II summarizes the respective optimization results.

TABLE I
40 mm × 40 mm AXIAL FANS CONSIDERED IN THE OPTIMIZATION.

Name	P / W	L / mm	m_{fan} / g	$\dot{V}_{\max}$ / dm³/s	$\Delta p_{\max}$ / Pa
GM0504PEV2-8.GN	0.4	6	7.5	2.6	20.0
MC19660	0.5	6	7.5	2.8	25.0
BP402012H-W	1.9	20	40.0	4.0	51.7
1608VL-04W-B60-B00	1.6	20	40.0	5.4	99.3
412JHH	3.3	25	50.0	6.7	216.3
9L0412J301	3.7	28	55.0	8.5	205.1
9GA0412P6G001	2.8	20	35.0	7.1	319.2
9GV0412P3K03	10.1	28	50.0	12.7	416.2
1611FT-D4W-B86-B50	11.4	28	49.0	13.8	736.9
1619FT-04W-B86-B50	12.6	48	71.0	14.1	800.0

TABLE II
OPTIMIZATION RESULTS. ($d = 3\,\text{mm}$, $t \in [1\,\text{mm}, 2\,\text{mm}]$, $\delta t = 0.1\,\text{mm}$, $c_{\text{MIN}} = 10\,\text{mm}$)

	MV side NPC	LV side fb	Transformer and ind.
$R_{\text{th,S-a,max}}$	1.25 K/W	1.10 K/W	0.46 K/W
$R_{\text{th,S-a}}$	1.241 K/W	1.097 K/W	0.444 K/W
m_{cs}	61 g	65 g	116 g
n	8	8	11
c	17 mm	20 mm	17 mm
fan	MC19660	MC19660	9GA0412P6G001
L	60 mm	60 mm	80 mm
b	40 mm	40 mm	40 mm
t	1 mm	1 mm	1 mm

B. Optimal Fin Length

The cooling system of Fig. 3(b) adds an air duct between the fan and the heat sink and, thus, allows a variable fin length of the heat sink. An air duct built of light weight materials can be beneficial, because a reduction of the fin length reduces the weight of the heat sink, decreases the average thermal resistance of the fin, $R_{\text{th,fin}}$, and increases the velocity of the air inside the channels, which, in turn increases the transfer coefficient h between the Aluminum channel walls and the air. A reduction of the fin length, however, reduces the effective surface of the fin, which counteracts the decrease of the thermal resistance between the fin and the air. The air duct, finally, causes an additional pressure drop and a slight increase of the total weight and volume of the heat sink system. With the model the impact of the air duct can be easily analyzed.

Fig. 11 depicts the total weights of optimized cooling systems with $A_{\text{hs}} = 40\,\text{mm}$ x $60\,\text{mm}$, $c_{\text{min}} = 37\,\text{mm}$ for 4 different fans and different values of $R_{\text{th,S-a,max}}$; steps occur in the plots as a result of the discrete number of channels, n. According to these results, the low power fans (MC19660 and GM0504PEV2-8.GN) yield lighter cooling systems for $R_{\text{th,S-a,max}} > 0.5\,\text{K/W}$ due to the lower weights of the fans. These fans, however, fail to realize cooling systems with low thermal resistances, i.e. no solutions result for $R_{\text{th,S-a,max}} < 0.5\,\text{K/W}$, due to limited air flow capabilities. The fans 9GA0412P6G001 ($P_{\text{fan}} = 2.76\,\text{W}$) and 1611FT-D4W-B86-B50 ($P_{\text{fan}} = 11.4\,\text{W}$) cause the total weight to increase for $R_{\text{th,S-a,max}} > 0.6\,\text{K/W}$ and are, thus, better suited for low maximum thermal resistances, $R_{\text{th,S-a,max}} < 0.6\,\text{K/W}$.

Fig. 12 shows the total weights of the same cooling systems with the optimal fin lengths being selected. The extended cooling system model clearly indicates the combination of heat sink and fan, which results in the minimum weight cooling system, e.g. the 9GA0412P6G001 fan is the optimal combination for $0.35\,\text{K/W} < R_{\text{th,S-a,max}} < 0.65\,\text{K/W}$. A comparison of Figs. 11 and 12 reveals the weight reduction achievable with the extended cooling system model, e.g. for $R_{\text{th,S-a,max}} = 0.5\,\text{K/W}$ the total weight is reduced by 14 % (97 g instead of 113 g).

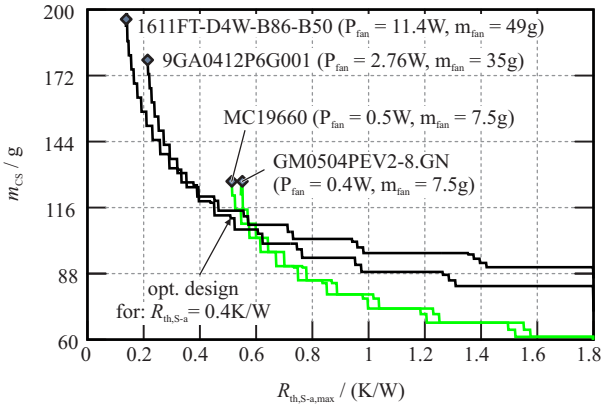

Fig. 11. Optimization results for $R_{\text{th,S-a,max}} \in [0, 1.8]$ K/W considering 4 fans, $A_{\text{hs}} = 40\,\text{mm}$ x $60\,\text{mm}$, $d = 3\,\text{mm}$, and fin length constrained to $c = 37\,\text{mm}$.

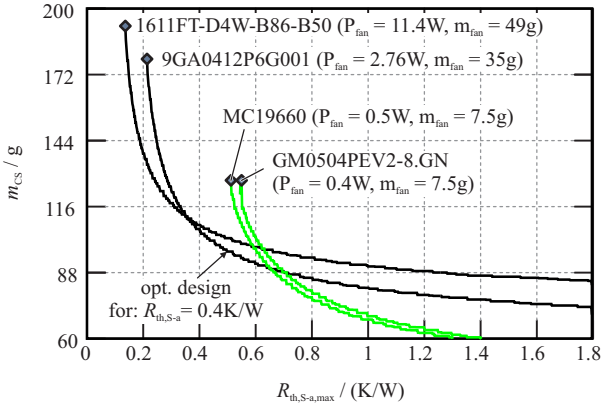

Fig. 12. Optimization procedure results for $R_{\text{th,S-a,max}} \in [0, 1.8]$ K/W considering 4 fans, $A_{\text{hs}} = 40\,\text{mm}$ x $60\,\text{mm}$, $d = 3\,\text{mm}$ and fin length optimization.

V. EXPERIMENTAL RESULTS

Twelve experimental cooling systems were used to verify the theoretical considerations presented above. The twelve cooling systems consist of three different heat sinks featuring the same base plate thicknesses, $d = 3\,\text{mm}$, and fin breaths, $t = 1\,\text{mm}$. The heat sinks differ in length, fin length and number of channels $\{L, c, n\} = \{\{80\,\text{mm}, 37\,\text{mm}, 13\}, \{60\,\text{mm}, 37\,\text{mm}, 8\}, \{60\,\text{mm}, 25\,\text{mm}, 9\}\}$. The thermal resistances of each heat sink are measured in combination with 4 different fans (GM0504PEV2-8.GN, MC19660, 9GA0412P6G001, 1611FT-D4W-B86-B50) to obtain twelve cooling systems.

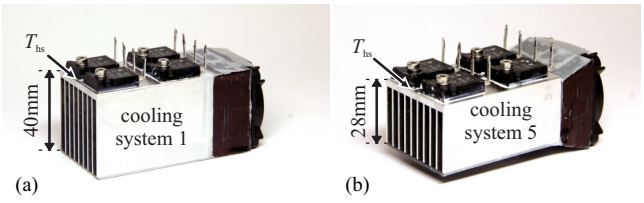

Fig. 13. Pictures of the realized cooling systems. T_{hs} indicates the location for the temperature measurement.

Four $100\,\Omega$ resistors are mounted to the base plates of each heat sink in order to provide defined heat fluxes. The base plate temperatures, T_{hs}, are measured at the surfaces as indicated in Figs. 13(a) and (b) with type K thermocouples. The cooling system is mounted on a hollow card board box and covered with thermally insulating material to reduce measurement errors due to heat conduction to the supporting table, natural convection, and radiation.

Fig. 14 summarizes the results obtained from measurements, FEM simulations, the proposed analytical model, and the model detailed in [6]. The mean deviations are 19.5% for FEM, 8% for the new model and 58% for the model of [6]. The measurement results demonstrate an excellent matching of calculated and measured results for the realized cooling systems, in particular in comparison to FEM simulation result accuracies. With comparable accuracies of an analytical model and FEM simulation results, the great difference only lies in the computational time, where an analytical model will produce a result within seconds on a personal computer and FEM simulations may require hours to produce the same results.

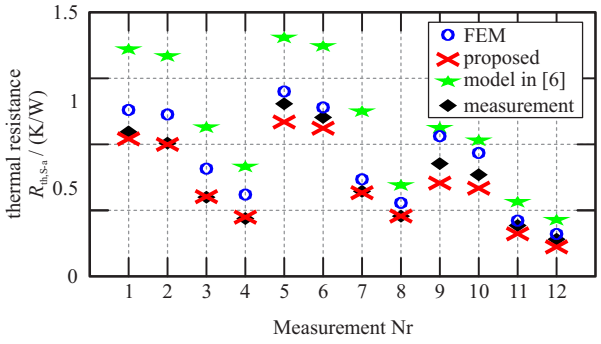

Fig. 14. Comparison of measurements (black diamonds) to the results obtained from FEM simulations (blue dots), the cooling system model given in [6] (green stars) and proposed cooling system model (red crosses).

VI. Conclusion

This Paper presents a weight optimization procedure for forced convection cooling systems that are composed of an extruded fin heat sink and a fan. It details the optimization of the number of air channels employed and the heat sink's fin thickness and length with respect to minimum weight. Furthermore, the selection of a suitable fan, which yields minimum total weight of the cooling system, is presented. An analytical cooling system model is detailed and compared to the results obtained from FEM simulations and from an existing cooling system model detailed in [6].

The presented experimental results document the effectiveness of the proposed cooling system model and optimization procedure. A comparison of a selected experimental cooling system with $R_{\text{th,S-a}} = 0.98\,\text{K/W}$ and $m_{cs} = 75\,\text{g}$ to commercially available products, of equivalent thermal resistance $R_{\text{th,S-a}} \approx 1\,\text{K/W}$, e.g. miniature cooling aggregate LAM 4 with heat sink dimensions of $40\,\text{mm} \times 40\,\text{mm} \times 60\,\text{mm}$ and total weight $m_{\text{cs}} = 157\,\text{g}$, reveals a weight reduction of $52\,\%$.

References

[1] J. W. Kolar, T. Friedli, F. Krismer, A. Looser, M. Schweizer, P. Steimer, and J. Bevirt, "Conceptualization and multi-objective optimization of the electric system of an airborne wind turbine," Proc. of the 20th IEEE International Symposium on Industrial Electronics (ISIE 2011), Gdansk, Poland, 27–30 June 2011, pp. 32–55.

[2] R. A. Friedemann, F. Krismer, J. W. Kolar, "Design of a minimum weight dual active bridge converter for an airborne wind turbine system," Proc. of the 27th Applied Power Electronics Conference and Exposition (APEC 2012), Orlando, Florida, USA, 5–9 Feb. 2012, pp. 509–516.

[3] M. B. Dogruoz and M. Arik, "On the conduction and convection heat transfer from lightweight advanced heat sinks," IEEE Transactions on Components and Packaging Technology, vol. 33, no. 2, pp. 424–431, June 2010.

[4] S. Lee, "Optimum design and selection of heat sinks," IEEE Transactions on Components, Packaging and Manufacturing Technology—Part A, vol. 18, no. 4, pp. 812–817, Dec. 1995.

[5] M. F. Holahan, "Fins, fans, and form: volumetric limits to air-side heatsink performance," IEEE Transactions on Components and Packaging Technology, vol. 28, no. 2, pp. 255–262, June 2005.

[6] U. Drofenik, A. Stupar, and J. W. Kolar, "Analysis of theoretical limits of forced-air cooling using advanced composite materials with high thermal conductivities," IEEE Transactions on Components, Packaging and Manufacturing Technology, vol. 1, no. 4, pp. 528–535, April 2011.

[7] R. J. Moffat, "Medeling Air-Cooled Heat Sinks as Heat Exchangers," 23rd Annual IEEE Semiconductor Thermal Measurement and Management Symposium (SEMI-THERM 2007), San Jose, CA, 18–22 Mar. 2007, pp. 200–207.

[8] Y. S. Muzychka, "Generalized Models for Laminar Developing Flows in Heat Sinks and Heat Exchangers," Heat Transfer Engineering, vol. 34, no. 2–3, pp. 178–191, 2013.

[9] P. Teertstra, M. M. Yovanovich, J. R. Culham, T. Lemczyk, "Analytical forced convection modeling of plate fin heat sinks," Fifteenth Annual IEEE in Semiconductor Thermal Measurement and Management Symposium, pp. 34–41, March 1999.

[10] Y. S. Muzychka, M. M. Yovanovich "Laminar Forced Convection Heat Tranfer in the Combined Entry Region of Non-Circular Ducts," ASME Transactions, vol. 126, pp. 54–61, February 2004.

[11] F. M. White, *Fluid Mechanics*, 4th ed. McGraw-Hill Series in Mechanical Engineering.

[12] Y. Shabany, *Heat transfer: thermal management of electronics*, Taylor & Francis, ISBN 978-1-4398-1467-3, pp. 281–283, 2009.

[13] J. R. Culham, W. A. Khan, M. M. Yovanovich, Y. S. Muzychka, "The influence of material properties and spreading resistance in the thermal design of plate fin heat sinks," Transactions–American Society of mechanical engineers, Journal of Electronics Packaging, vol. 129, no. 1, 2007.

[14] Y. S. Muzychka, M. M. Yovanovich "Pressure drop in laminar developing flow in noncircular ducts: a scaling and modeling approach,"Journal of Fluids Engineering, vol. 131, no. 11, pp. 111105, November 2009.

[15] W. Kays, M. Crawford, B. Weigand, *Convective Heat and Mass Transfer*, McGraw-Hill, ISBN 978-0-0712-3829-8, 1977.

[16] Verein Deutscher Ingenieure, *VDI-Wärmeatlas* (in German), 10th ed. Berlin: Springer, 2006, p. 945.

[17] ASHRAE Research, *Fundamentals: 2005 Ashrae Handbook : Si Edition*, Amer Society of Heating, ISBN 978-1-9318-6271-4, ch. 35–36, 2005.